Discover Pharmaceutical Sciences

RESEARCH Open Access

In silico evaluation of N-methyl-1-adamantaneacetamide and 3′,4′-di-O-methyl ellagic acid-4α-La-rhamnopyranoside from *Asystasia gangetica* and *Synadenium glaucescens pax* as potential antidiabetic agents

Nawazi M. Kagimbo[1*], Christopher J. Mwankuna[1] and Faith P. Mabiki[1]

*Correspondence:
Nawazi M. Kagimbo
nawazimatsawili@gmail.com
[1]Department of Chemistry and Physics, College of Natural and Applied Sciences, Sokoine University of Agriculture, Morogoro, Tanzania

Abstract

Background Type 2 diabetes mellitus (T2DM) remains a worldwide health issue, requiring the development of new therapeutic agents with better effectiveness and safety. Plant-based compounds show promising potential, and computational methods allow efficient evaluation of their pharmacological properties.

Methodology This study used molecular docking, ADME prediction, and molecular dynamics simulations to assess secondary metabolites from *Asystasia gangetica* and *Synadenium glaucescens pax* against important diabetic targets, including PPARγ, 11β-HS1, DPP4, and SGLT2.

Results In silico analysis of secondary metabolites from *A. gangetica* and *S. glaucescens pax* identified 15 compounds likely to interact with selected proteins involved in blood sugar regulation. N-methyl-1-adamantaneacetamide and benzyl β-D-glucopyranoside demonstrated favourable ADME properties and showed strong binding energies. The highest binding energy observed was − 182.32 ± 11.49 kJ/mol with 3′,4′-di-O-methyl ellagic acid-4α-L-rhamnopyranoside in the PPAR system. Additionally, despite its robust van der Waals and electrostatic interactions, the considerable positive polar solvation energy notably affected the overall binding energy of 3′,4′-di-O-methyl ellagic acid-4α-L-rhamnopyranoside. Conversely, the lower polar solvation energy of N-methyl-1-adamantaneacetamide improved its overall binding energy, making it the ligand with the most favourable total binding energy within the PPAR system.

Conclusion The in-silico analysis indicates that N-methyl-1-adamantaneacetamide from Asystasia gangetica and 3′,4′-di-O-methyl ellagic acid-4α-L-rhamnopyranoside from Synadenium glaucescens are promising multi-target compounds for blood sugar regulation. Molecular dynamics simulations favour N-methyl-1-adamantaneacetamide for the Pparγ receptor and 3′,4′-di-O-methyl ellagic acid-4α-L-rhamnopyranoside for the SGLT2 receptor as the most effective ligands owing to their optimal binding

properties and stability. Further experimental validation is necessary to evaluate their potential efficacy as antidiabetic drugs in vitro and in vivo.

Keywords Blood sugar disorder, *Asystasia gangetica*, *Synadenium glaucescens*, Swiss ADME, Autodock vina, Molecular dynamic simulation

1 Background

Blood sugar disorder is a metabolic disease primarily characterised by elevated blood sugar levels caused by insufficient or resistant insulin production. It is a metabolic illness now sweeping across the globe [1]. About 90% of blood sugar disorders are attributed to type 2 diabetes, the most common form of the disease. Type 2 diabetes, also known as non-insulin-dependent diabetes, is the leading cause of chronic metabolic conditions [2]. Globally, the prevalence of T2DM has surged, affecting over 537 million adults as of 2021, with projections estimating this number will exceed 783 million by 2045 [3]. Orally administered medications for blood sugar disorders use various modes of action, such as activating or inhibiting drug receptors, eliciting distinct physiological responses [4]. Additionally, the development of undesirable side effects such as hypoglycemia, weight gain, nausea, gastrointestinal issues, hepatotoxicity, and diarrhoea has been associated with existing medications.s, hepatotoxicity, and diarrhoea have been associated with the existing medications [4, 5].

Computational methods are among the holistic ways to discover new compounds with potential medicinal applications. Recent studies have extensively employed computational techniques to investigate potential antidiabetic agents, reflecting an innovative approach to phytochemical screening. One key study used gas chromatography-mass spectrometry (GC–MS) combined with molecular docking to analyse the methanolic extract of Hunteria umbellata, identifying its bioactive compounds that showed substantial anti-diabetic potential. The findings indicated that compounds from Hunteria umbellata interacted favourably with key therapeutic targets involved in glucose metabolism, thereby highlighting the plant as a promising phytotherapeutic candidate [6]. Similarly, research employing in silico molecular docking studies has examined various phytochemicals against dipeptidyl peptidase-4 (DPP-4), screening multiple phytochemical structures and revealing significant interactions with the active sites of DPP-4, paving the way for future developments in natural product pharmacology [7]. Another notable investigation assessed the antidiabetic potential of phenolic compounds derived from blue corn (*Zea mays L.*) and black bean (*Phaseolus vulgaris L.*). In silico modelling demonstrated the binding affinity of these compounds to critical metabolic enzymes, suggesting their important role in glycemic control [8]. Studies like these highlight the multifaceted roles of phenolic compounds in diabetes management, encouraging further exploration of their therapeutic applications. Likewise, the antimicrobial and anti-diabetic phytochemical erythrin has also been subjected to in silico analysis against therapeutic targets for diabetes. The results underscored its potential as a therapeutic agent, opening avenues for further research into its mechanism of action and clinical efficacy [9]. Collectively, these studies emphasise the usefulness of molecular docking and computational approaches in discovering and validating novel anti-diabetic compounds.

Against this backdrop, ethnopharmacological records indicate that *Asystasia gangetica* leaves are used in East African folk medicine for glycemic control [10], while ellagic acid derivatives from *Synadenium glaucescens* exhibit potent anti-inflammatory

and antioxidant activity relevant to T2DM pathogenesis [11]. Both *Asystasia gangetica* and *Synadenium glaucescens* have provided a rich source of secondary metabolites with potential therapeutic benefits, including anti-diabetic activity [12] using extracts of *A. gangetica*, anti-Newcastle disease [13–16], antibacterial [17, 18], and antiviral [15, 16]. The decision to focus on these medicinal plants stems from their unique secondary metabolites, including 3′,4′-di-O-methyl ellagic acid-4α-L-rhamnopyranoside isolated from *S. glaucescens*, as its derivatives are recognised for their anti-oxidative and anti-inflammatory properties, which contribute to managing type 2 diabetes [19, 20]. Through in silico analysis, the research aims to evaluate the binding efficacy of secondary metabolites from *A. gangetica* and *S. glaucescens* against key enzymes and receptors involved in glucose metabolism.

2 Methods

2.1 Protein selection and preparation

A comprehensive literature review was conducted to identify proteins implicated as therapeutic targets for blood sugar regulation, guiding our study's subsequent selection of proteins. Proteins were chosen based on their current clinical relevance in T2DM and druggability, as indicated in Table 1. Crystal structures were obtained from RCSB PDB (8HEZ, 1J2E, 1BHS, 1PRG) and prepared by removing water molecules, adding polar hydrogens, and assigning Kollman charges (https://www.rcsb.org/), ensuring the structu ral authenticity and reliability of the proteins for subsequent docking analyses.

Table 1 Selected protein-based approaches for blood sugar control

S/N	Protein	Action mode	Function	References
1	Protein tyrosine phosphatase	Inhibitor (dephosphorylation)	Regulates phosphorylation by removing phosphate from tyrosine residues	Genovese [21]
2	Protein kinase B	Activator (phosphorylation)	Involved in cell survival, growth, and metabolism	Teimouri et al. [22]
3	Insulin receptor substrate	Activator (phosphorylation)	Mediated insulin signalling	Batista et al. [23]
4	AMP-activated protein kinase	Activator (phosphorylation)	Regulates energy homeostasis and metabolism	Haye et al. [24]
5	11β-hydroxysteroid Dehydrogenase 1	Inhibitor (cortisol production)	Converts active cortisol to inactive cortisone	Gregory et al. [25]
6	Glucose transporter	Activator (glucose uptake)	Facilitates glucose transport across cell membranes	Berger and Zdzieblo [26]
7	Peroxisome Proliferator-Activated Receptor gamma	Activator (gene expression)	Regulates lipid metabolism and insulin sensitivity	Mishra et al. [27]
8	Interleukin-1-associated kinase	Activator (inflammatory signaling)	Involved in immune responses	Kondo et al. [28]
9	Fructose 1,6-bisphosphatase	Inhibitor (glucose production)	Regulates gluconeogenesis	Xu et al. [29]
10	Dipeptidyl peptidase IV	Inhibitor (increased GLP-1 levels)	Cleaves incretin hormones	Deacon [30]
11	Glutamine fructose-6-phosphate amidotransferase	Activator (glucose metabolism)	Involved in hexosamine biosynthesis	Oliveira et al. [31]
12	Sodium-glucose transport 2	Inhibitor (glucose excretion)	Reabsorbs glucose in the kidneys	Provenzano et al. [32]

2.2 Ligand selection and preparation

Ligand selection involved isolated compounds from *A. gangetica* [33] and *S. glaucescens pax* using Swiss Target Prediction (http://www.swisstargetprediction.ch/) and ChEMBL (https://www.ebi.ac.uk/chembl/), focusing on their potential interactions with key proteins related to blood sugar regulation. Compounds were retrieved and their 3D structures refined from PubChem (https://pubchem.ncbi.nlm.nih.gov/), enabling their suitability for further molecular docking studies. The selection was based on whether the compound is active or inactive, but reaches the threshold that allows it to be predicted with the target or its homologs, showing similarity to the query molecule based on similarity measures. Empagliflozin, Dapagliflozin, Linagliptin, Saxagliptin, Pioglitazone, and Rosiglitazone served as standard ligands for secondary metabolites targeting SGLT-2, Dpp4, and Pparγ.

2.3 ADME predictions

Absorption, Distribution, Metabolism, and Excretion predictions (ADME) were performed using Swiss ADME (http://www.swissadme.ch/index.php) to evaluate the ADME properties of the identified ligands. The resulting data provided valuable insights into the pharmacokinetic profiles of these ligands. This information was utilised to assess their bioavailability and potential as drug candidates for blood sugar treatment [34].

2.4 Molecular docking

Chimera and AutoDocktool (chimera-1.17.3-win64.exe and autodock_vina_1_1_2_win32.msi) were used to perform the docking analysis of the candidate compounds with selected target proteins. With other options set to default, this tool was run using a search grid centred on the protein with a box spacing of: 70.0, 69.0, 75.0 and size: 56.0, 66.0, 76.0 for 8hez; centre: 49.0, 59.0, 32.0 and size: 70.0, 67.0, 83.0 for 1j2e; centre: 15.0, 3.0, − 2.0 and size: 53.0, 45.0, 60.0 for 1bhs and 1prg; with centre: 13.0, 57.0, 20.0 and size: 47.0, 53.0, 60.0 for the latter. Grid centres and sizes were set to encompass the co-crystallised ligand sites. The compounds were docked into the selected protein crystal structures, which involved removing water molecules and nonpolar hydrogen atoms, and adding polar hydrogen atoms. For each compound, the position with the most significant score was selected. Docking simulations were performed with the exhaustiveness parameter set to 8, while all other settings remained at their default values. Method reliability was validated by redocking the co-crystallized ligand, yielding a root-mean-square deviation (RMSD) of ≤ 2 Å from the experimental pose. The most stable conformation of each molecule for binding to the active site of the selected protein was considered the optimal docking pose.

2.5 Molecular dynamics

2.5.1 System separation

After docking and ADMET predictions, the top candidates were filtered and chosen for further analysis. Receptors with strong binding energies were selected for MD simulations.

2.5.2 Molecular dynamics simulations

GROMACS version 2020.1 [35] was used to perform MD simulations. The receptor structures were defined using the CHARMM36 force field for all protein atoms [36]. Since the non-bonded parameters for ligands were absent in the force field, the Swissparam server [37] was employed to generate a ligand topology compatible with the receptor's protein force field. The topologies were combined to create a complex starting structure, which was solvated with the TIP3P water model [38] within a cubic box measuring x, y, and z. The solvated systems underwent energy minimisation using the steepest descent algorithm [39]. For 50,000 steps with a convergence force tolerance of 1000 kJ/mol. The systems were then equilibrated in two stages: first, a 500 ps NVT equilibration with a V-rescale thermostat [39], followed by a 500 ps NPT equilibration with a Parrinello-Rahman barostat [40]. The MD simulation was conducted for 100 ns, maintaining 1 bar pressure with a Parrinello-Rahman barostat and a velocity-rescale thermostat set at 300 K. Hydrogen bonds were constrained using LINC algorithms [41]. Electrostatic and van der Waals interactions were truncated at a cut-off of 1.4 nm, with Particle Mesh Ewald employed to handle electrostatic interactions and to scale the van der Waals forces, interactions were set at a cut-off of 1.4 nm. Electrostatic interactions, particle Mesh Ewald was used to scale the van der Waals interaction values.

2.5.3 Ligand preparation

After docking analysis, the most stable shape with the optimal docking pose was chosen. It was assigned Gasteiger charges and optimised using Avogadro software to reach an energy-preferred conformation.

2.5.4 Protein preparation

The 3D structures of selected proteins were obtained in Structural Data File (SDF) format from RCSB Protein Data Bank (https://www.rcsb.org/). Solvent molecules and other heteroatoms were removed from the protein structures. Missing residues were added to the receptors to ensure completeness. Kollman charges and polar hydrogen atoms were assigned to the structures to achieve neutrality. The final structures were converted to PDB format and are now ready for docking.

3 Results

3.1 Identification of selected proteins

Twelve proteins are shown in Table 1 SGLT-2, DPP4, 11β-HS1, and PPARy were selected as therapeutic targets for blood sugar regulation based on their biomarker potential, drug availability, and development. These proteins have played a key role in drug design efforts to tackle blood sugar disorders by inhibiting or activating their respective receptors [9, 42]. The 3D structures of these proteins were retrieved, and their PDB codes (8hez for SGLT-2, 1j2e for DPP4, 1bhs for 11β-HS1, and 1prg for PPARy) were obtained from the RCSB Protein Data Bank.

3.2 Criteria for ligand selection

The selection of ligands was conducted using Swiss Target Prediction and ChemBL. Approximately 135 compounds were predicted, with only 15 compounds from *A. gangetica* and *S. glaucescens pax* meeting the criteria for potential interaction with proteins

involved in blood sugar regulation, as indicated in Table 2. Compounds 1–13 and 15 were identified from *A. gangetica*, while compound 14 originated from *S. glaucescens pax*. Compounds 16–21 were standard compounds for the selected set. According to ChEMBL results, compounds 6, 7, 12, and 16–19 were predicted to be active on their targets with varying confidence levels. A confidence level of 70% indicates moderate confidence but acknowledges some uncertainty; 80% reflects a higher confidence level than 70%, and 90% implies greater confidence with lower uncertainty. Other compounds are inactive or show mixed activity but are predicted to interact with the selected target based on the enabled threshold. In contrast, some compounds, such as 2, 4, 9, 11, and 14, are not identified in CHEMBL. On Swiss Target Prediction, compounds 2, 3, 5, 10, and 13 showed relative probabilities ranging from 0.0429 to 0.1115 compared to standard compounds 16–21. Their probabilities, influenced by similarity measures (2D/3D), ranged from 0.9388 to 1, which enhances the accuracy of target prediction; other compounds exhibited a probability of zero, as shown in Table 2. Regarding Sglt-2, Empagliflozin and Dapagliflozin; Dpp4 inhibitors like Linagliptin and Saxagliptin; and PPARy modulators such as Pioglitazone and Rosiglitazone were used as standard inhibitors and modulators, based on their mechanisms of action, since they are used in blood sugar control.

3.3 Evaluation of ADME and drug-likeness

The pharmacokinetics and drug-likeness properties of selected compounds are detailed in Tables 3 and 4. These compounds' log Pow (octanol–water partition coefficient) ranges from − 1.85 to 7.24, with higher values indicating increased hydrophobicity. Compounds 2, 3, 4, 10, 11, 13, and 16–21 exhibit higher hydrophobicity, suggesting enhanced lipid solubility. Log S (aqueous solubility (ESOL, Ali, and SILICOS-IT) for the selected compounds spans from − 7.90 to − 0.24, where lower values denote decreased solubility and potential impact on drug absorption. Compounds 1–10, 12, 14–16, and 19 display good water solubility, implying a possible influence on drug absorption. All compounds show high gastrointestinal (GI) absorption, except for compounds 5–7 and 12–14, which exhibit low GI absorption. High GI absorption indicates efficient uptake from the gastrointestinal tract. Regarding blood–brain barrier (BBB) permeation, most compounds, apart from 2 to 4, 8, 10, and 11, do not cross the BBB, suggesting limited central nervous system activity for most. The majority of compounds are substrates for P-gp (P-glycoprotein), except for 1–4, 8–11, 13–15, 20, and 21, which could influence their bioavailability when CYP inhibitors (Cytochrome P450 inhibitors) are present. Some compounds show potential to inhibit various CYP isoforms (1A2, 2C19, 2C9, 2D6, and 3A4). Nonetheless, compounds 1, 4–10, 12–15, and 18 are non-inhibitors for all CYP isoforms, playing a significant role in drug metabolism. Around half of the clearance of typical clinical medications can be attributed to one or more CYP enzymes [43]. Predicted compounds' Log Kp (skin permeation) ranges from − 10.91 to − 2.20, with higher negative values indicating better skin permeation potential, as illustrated in Table 3.

Regarding drug-likeness, most compounds conform to Lipinski's Rule of Five, with some violations such as having too many hydrogen bond donors or acceptors (NH or OH > 5) However, compounds 7 and 12 are exceptions, with multiple violations including exceeding a molecular weight of 500, having more than ten rotatable bonds (N or O), and possessing (NH or OH) > 10. Additionally, most compounds pass Ghose's filter,

Table 2 Predicted ligands using ChemBl and SwissTargetPrediction

S/N	Compound name	CHEMBL ID	PubChem CID	Target protein	Organism	ChemBL			Swiss target prediction	
						Status			Probability	Known actives (3D/2D)
						70%	80%	90%		
1	Salidroside	465208	159278	SGLT-2	Hs	E	E	B	0.0	78/82
				DPP4	Hs	I	I	I	0.0	1/0
					Rn	E	I	I		
				PPARγ	Hs	I	I	I	-	-
2	4-methoxy-3-(-quinolinyloxymethyl) benzaldehyde	–	590877	11β-HS1		–	–	–	0.1115	23/0
				PPARγ		–	–	–	0.1115	47/0
3	Manool	4162501	3034394	SGLT-2	Hs	I	I	I	–	–
				DPP4	Hs	I	I	I	–	–
					Rn	I	I	I		
				PPARγ	Hs	I	I	I	–	–
				11β-HS1		–	–	–	0.1473	164/17
4	2-Phenazine carboxylic acid	–	614224	PPARγ	–	–	–	–	0.0	37/0
5	(6S,9R)-reseoside	482383	9930064	SGLT-2	Hs	I	I	I	0.1133	463/0
				DPP4	Hs	E	E	B	–	–
					Rn	E	E	I		
				PPARγ	Hs	I	I	I	–	–
6	Ajugol	3810218	6325127	SGLT-2	Hs	I	I	I	0.0	92/0
				DPP4	Hs	E	A	A	0.0	1/0
					Rn	E	I	I		
				PPARγ	Hs	I	I	I	–	–
7	Rhoifloin	395990	5282150	SGLT-2	Hs	A	A	A	–	–
				DPP4	Hs	I	I	I	–	–
					Rn	E	E	I		
				PPARγ	Hs	I	I	I	–	–
8	Hydrazine (Phenyl-methyl)	1231544	11157	SGLT-2	Hs	I	I	B	–	–
				DPP4	Hs	I	I	I	0.0	2/0
					Rn	E	I	I		
				PPARγ	Hs	I	I	I	–	–
9	2-formyl-histamine	–	541600	DPP4	–	–	–	–	0.0	2/0
10	N-methyl-1-adamantaneacetamide	1424905	610088	DPP4	Hs	I	I	I	0.0429	0/85
					Rn	I	I	I		
				PPARγ	Hs	I	I	I	-	-
				11β-HS1		–	–	–	0.0715	241/41
				SGLT-2	Hs	I	I	I	–	–
11	5-methyl-2-phenylindolizine	–	610180	11β-HS1		–	–	–	0.0	11/0
12	Lonicerine	452979	5282152	SGLT-2	Hs	A	A	A	–	–
				DPP4	Hs	I	I	I	–	–
					Rn					
				PPARγ		E	I	I	–	–
13	B-sitosterol	221542	222284	SGLT-2	Hs	I	I	I	–	–
				DPP4	Hs	I	I	I	–	–
					Rn	I	I	I		
				PPARγ	Hs	I	I	I	0.1067	0/12
				11β-HS1		–	–	–	0.1062	11/23

Table 2 (continued)

S/N	Compound name	CHEMBL ID	PubChem CID	Target protein	Organism	ChemBL			Swiss target prediction	
						Status			Probability	Known actives (3D/2D)
						70%	80%	90%		
14	3′,4′-di-o-methyl ellagic acid-4α-l-rhamnopyranoside	–	–	DPP4	Hs	–	–	–	0.0	2/0
15	Benzyl β-D-glucopyranoside	2336738	13254166	SGLT-2	Hs	I	I	I	0.112	68/117
				DPP4	Hs	I	I	I	0.112	2/0
					Rn	I	I	I		
				PPARγ	Hs	I	I	I	–	–
16	Empagliflozin	2107830	11949646	SGLT-2	Hs	A	A	A	0.995	847/590
17	Dapagliflozin	429910	9887712	SGLT-2	Hs	A	A	A	1.0	895/650
18	Linagliptin	237500	10096344	DPP4	Hs	E	A	B	1.0	669/305
					Rn	E	E	I		
19	saxagliptin	385517	11243969	DPP4	Hs	A	A	A	0.9681	237/441
					Rn	I	I	I		
20	Pioglitazone	595	4829	PPARγ	Hs	I	I	I	0.9388	683/59
21	Rosiglitazone	121	77999	PPARγ	Hs	I	I	I	1	527/71

A, active (interact with target); I, inactive (not to interact with target); E, empty (model not able to predict the compound); B, both (could not conclude); Hs, homo sapiens; Rn, rattus norvegicus; PPARy, peroxisome proliferator activated receptor gamma; DPP4, dipeptidyl peptidase IV; SGLT-2, sodium-glucose transport protein 2 and 11β-HS1, 11ββ-hydroxysteroid dehydrogenase

except for a few that breach the criteria, such as molecular weight > 480 and several heavy atoms > 70, like compounds 1, 5–9, 12, 13, 15, and 18. Most compounds adhere to Veber's rule, which assesses rotatable bonds and the topological polar surface area (TPSA). However, some compounds (6, 7, 12, and 14) violate TPSA thresholds (> 140). Several compounds meet Egan's criteria, except for compounds 5–7 and 12–14, which have elevated TPSA values (> 131.6) and excessively high WLOGP values (> 5.88). Most compounds satisfy Muegge's criteria, though some violate rules regarding XLOGP, the number of heteroatoms, TPSA, and hydrogen bond acceptors and donors—such as compounds 3, 6–9, and 11–14. The bioavailability score ranges from 0.17 to 0.85, with higher scores indicating better-predicted bioavailability. Nonetheless, the results show that compounds 2, 4, 10, 16, 17, 19, 20, and 21 meet all drug-likeness properties, suggesting their potential for oral bioavailability in blood sugar control as shown in Table 4.

3.4 Molecular docking analysis

Docking was performed on fourteen compounds, except for compound 14, which remains unidentified in the compound's database. Compounds 8 and 9 exhibited the lowest binding among all predicted compounds, while the most significant energy for compounds 1, 2, 4, 7, 11, 12, and 13 was observed at 8hez, compared to the standard compounds 16 and 17. Compounds 7 and 12 showed the highest binding energy to 1j2e and 1prg. However, among the 15 compounds, compounds 1, 10, and 15 displayed moderate binding energy with the selected proteins when compared to the standards mentioned above, as indicated in Table 5.

Compound 1, 10, and 15 showed consistent molecular interactions with amino acid residues on target 8Hez: Phe 98, Ser 287, Asn 75, Gln 445, Ala 447, Gly 356, Gly 449, Cys 255, Ala 344, Cys 345, Ala 90, Phe 152, and Ser 177 for compound 1; Phe 152 and

Table 3 ADME properties of selected compounds

Compounds	Log Po/w	Log S			GI-absorption	BBB permeant	P-gp substrate	CYP1A2 inhibitor	CYP2C19 inhibitor	CYP2C9 inhibitor	CYP2D6 inhibitor	CYP3A4 inhibitor	Log Kp (skin permeation)
		ESOL	Ali	SILICOS-IT									
1	− 0.59	− 0.92	− 0.97	− 0.44	High	No	No	No	No	No	No	No	− 8.88 cm/s
2	2.98	− 3.72	− 3.62	− 6.43	High	Yes	No	Yes	Yes	Yes	Yes	Yes	− 6.00 cm/s
3	5.06	− 4.98	− 5.91	− 4.83	High	Yes	No	No	Yes	Yes	Yes	No	− 4.01 cm/s
4	2.12	− 3.13	− 3.12	− 4.38	High	Yes	No	Yes	No	No	No	No	− 6.13 cm/s
5	− 0.19	− 1.24	− 1.33	− 0.03	Low	No	Yes	No	No	No	No	No	− 9.40 cm/s
6	− 1.65	− 0.42	− 0.41	2.45	Low	No	Yes	No	No	No	No	No	− 9.98 cm/s
7	− 0.81	− 3.22	− 4.19	− 1.48	Low	No	Yes	No	No	No	No	No	− 9.94 cm/s
8	0.96	− 1.44	− 1.15	− 2.25	High	Yes	No	No	No	No	No	No	− 6.50 cm/s
9	− 0.31	− 0.38	− 0.24	− 1.61	High	No	No	No	No	No	No	No	− 7.71 cm/s
10	2.56	− 2.77	− 3.2	− 2.75	High	Yes	No	No	No	No	No	No	− 5.48 cm/s
11	3.67	− 4.71	− 4.51	− 5.37	High	Yes	No	Yes	Yes	No	Yes	No	− 4.23 cm/s
12	− 1.85	− 2.54	− 3.35	− 0.2	Low	No	Yes	No	No	No	No	No	− 10.91 cm/s
13	7.24	− 7.9	− 9.67	− 6.19	Low	No	No	No	No	No	No	No	− 2.20 cm/s
14	0.95	− 2.77	− 3.2	− 2.75	Low	No	No	No	No	No	No	No	− 8.89 cm/s
15	− 0.32	− 1.04	− 0.91	− 0.62	High	No	No	No	No	No	No	No	− 8.45 cm/s
16	1.97	− 3.80	− 3.94	− 4.25	High	No	Yes	No	No	No	Yes	No	− 7.61 cm/s
17	2.17	− 3.78	− 4.08	− 4.46	High	No	Yes	No	No	No	Yes	No	− 7.13 cm/s
18	1.97	− 4.11	− 3.99	− 4.99	High	No	Yes	No	No	Yes	No	Yes	− 7.83 cm/s
19	1.2	− 2.06	− 2.21	− 1.32	High	No	Yes	No	No	No	No	No	− 7.71 cm/s
20	3.09	− 4.31	− 5.41	− 6.78	High	No	No	Yes	Yes	Yes	Yes	Yes	− 5.81 cm/s
21	2.36	− 3.91	− 4.81	− 5.71	High	No	No	No	Yes	Yes	Yes	Yes	− 6.27 cm/s

Cys 255 for compound 15. Interactions with 1j2e included Ile 405, Phe 357, Arg 358, Glu 206, Thr 351, Trp 157, Met 348, Thr 350, and Ser 376 for compound 1; Asp 737 and Asn 92 for compound 10; and Phe 95, Trp 629, Ile 102, Trp 157, and Leu 504 for compound 15. For 1bhs, interactions involved Gly 92, Ile 14, Ser 12, Asn 90, Gly 9, Gly 15 for compound 1; Gly 15 for compound 10; and Ser 12, Gly 9, Gly 92, and Gly 141 for compound 15. With 1prg, the amino acid residues Arg 288, Glu 343, Ser 342, Lys 265, and Leu 340 interacted with compound 1; Lys 263 with compound 10; and Ser 342, Gly 284, Lys 265, and Lys 263 with compound 15. Stable binding interactions between the amino acid residues of targets 8hez, 1j2e, 1bhs, and 1prg and compounds 1, 10, and 15 are presented in Figs. 1, 2, 3.

3.5 Stability of diabetic receptors against ligands

The stability of the diabetic receptors after ligand addition, including root mean squared deviation, radius of gyration, and root mean squared fluctuations, was investigated as follows.

3.5.1 Root mean squared deviation

Root mean squared deviation (RMSD) measures how much a structure changes over time. RMSD calculates the average distance each atom has moved from its original position. It is commonly used in MD simulations to assess the stability of a molecule, such as a protein, after ligand binding. This study employed RMSD to review the stability and flexibility of the peroxisome proliferator-activated receptor (PPAR) following ligand binding, with results shown in Fig. 4A. RMSD values ranged from 0.2 to 0.35 nm, with the Benzyl β-D-glucopyranoside ligand displaying the lowest RMSD, averaging 0.20 nm over a 100 ns period. The N-methyl-1-adamantaneacetamide ligand maintained a consistent RMSD of 0.25 nm throughout the simulation. Another ligand, 3′,4′-di-O-methyl ellagic acid-4α-I-rhamnopyranoside, exhibited variable RMSD values, beginning at 0.20 nm for the first 20 ns, rising to 0.25 nm over the next 40 ns, reaching a peak of 0.3 nm at 60 ns, and then stabilising at 0.25 nm for the remainder of the simulation.

For the sodium-glucose cotransporter 2 (SGLT2) receptor, the RMSD profiles observed in Fig. 4B ranged from 0.20 to 0.25 nm. The 3′,4′-di-O-methyl ellagic acid-4α-I-rhamnopyranoside showed the lowest and most stable RMSD, maintaining a distance of 0.20 nm, similar to the benzyl β-D-glucopyranoside ligand. The N-methyl-1-adamantaneacetamide ligand exhibited a slightly larger RMSD value than the other ligands mentioned earlier.

3.5.2 Radius of gyration

The radius of gyration (Rg) indicates how spread out the atoms of a molecule are, similar to a protein around its centre of mass. It helps us understand the overall size and compactness of the molecule. A stable protein typically maintains a specific level of compactness, shown by a consistent Rg. A more compact structure has a smaller Rg, which suggests the protein is properly folded and stable. The study examined the Rg values to evaluate the stability and compactness of the sodium-glucose cotransporter 2 (SGLT2) receptor after ligand binding. Figure 5A demonstrates that the new compound (3′,4′-di-O-methyl ellagic acid-4α-I-rhamnopyranoside) and N-methyl-1-adamantaneacetamide ligand sustained an Rg of 1.95 nm throughout the 100 ns simulation, indicating

Table 4 Drug-likeness properties of selected compounds

Compound	Lipinski	Ghose	Veber	Egan	Muegge	Bioavailability score
1	Yes	No	Yes	Yes	Yes	0.55
2	Yes	Yes	Yes	Yes	Yes	0.55
3	Yes	Yes	Yes	Yes	No	0.55
4	Yes	Yes	Yes	Yes	Yes	0.85
5	Yes	No	Yes	No	Yes	0.55
6	Yes	No	No	No	No	0.55
7	No	No	No	No	No	0.17
8	Yes	No	Yes	Yes	No	0.56
9	Yes	No	Yes	Yes	No	0.55
10	Yes	Yes	Yes	Yes	Yes	0.55
11	Yes	Yes	Yes	Yes	No	0.55
12	No	No	No	No	No	0.17
13	Yes	No	Yes	No	No	0.55
14	Yes	Yes	No	No	No	0.55
15	Yes	No	Yes	Yes	Yes	0.55
16	Yes	Yes	Yes	Yes	Yes	0.55
17	Yes	Yes	Yes	Yes	Yes	0.55
18	Yes	No	Yes	Yes	Yes	0.55
19	Yes	Yes	Yes	Yes	Yes	0.55
20	Yes	Yes	Yes	Yes	Yes	0.55
21	Yes	Yes	Yes	Yes	Yes	0.55

Table 5 Docking results of selected compounds on their target proteins

Tool	Chimera and Autodock vina				Active tension
Compound	Binding score (Kcal/mol)				
	8HEZ	1JF2E	1BHS	1PRG	
1	−9.2	−7.3	−7.6	−7.6	10
2	−9.6	−7.1	−8.4	−8.6	5
3	−6.9	−7.0	−7.5	−8.5	5
4	−8.8	−7.5	−7.6	−8.6	2
5	−7.6	−7.8	−8.4	−7.9	10
6	−7.9	−7.6	−7.6	−7.3	9
7	−9.7	−9.2	−10.0	−11.0	14
8	−6.4	−5.8	−5.5	−5.9	3
9	−5.3	−5.1	−5.0	−4.8	4
10	−7.7	−6.8	−6.4	−7.0	2
11	−8.8	−7.7	−7.5	−9.3	1
12	−9.8	−9.3	−9.8	−10.7	15
13	−9.3	−8.8	−9.7	−9.3	7
14	–	–	–	–	–
15	−7.1	−6.8	−7.1	−7.3	8
16	−8.5	–	–	–	10
17	−7.9	–	–	–	10
18	–	−9.1	–	–	5
19	–	−8.0	–	–	4
20	–	–	–	−9.6	7
21	–	–	–	−8.9	7

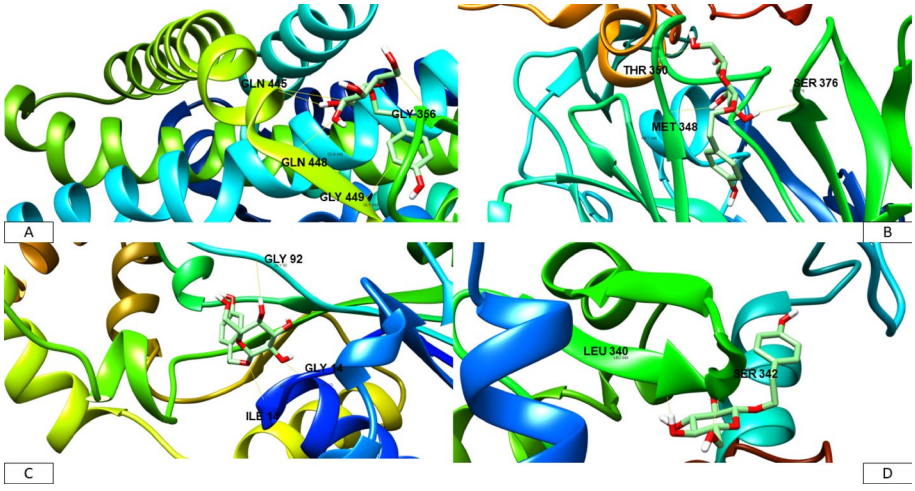

Fig. 1 A stable interaction between compound 1 and **A** 8hez, **B** 1j2e, **C** 1bhs, and **D** 1prg

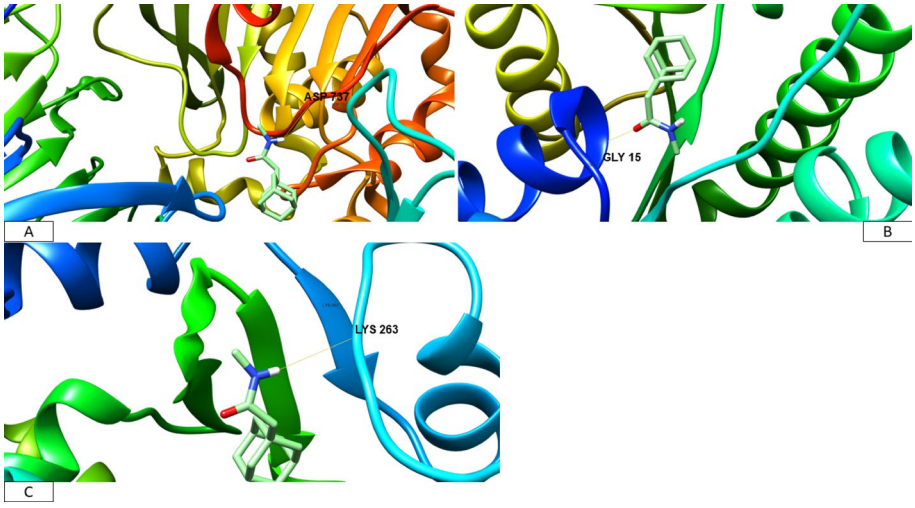

Fig. 2 A stable interaction between compound 10 and **A** 1j2e, **B** 1bhs, and **C** 1prg

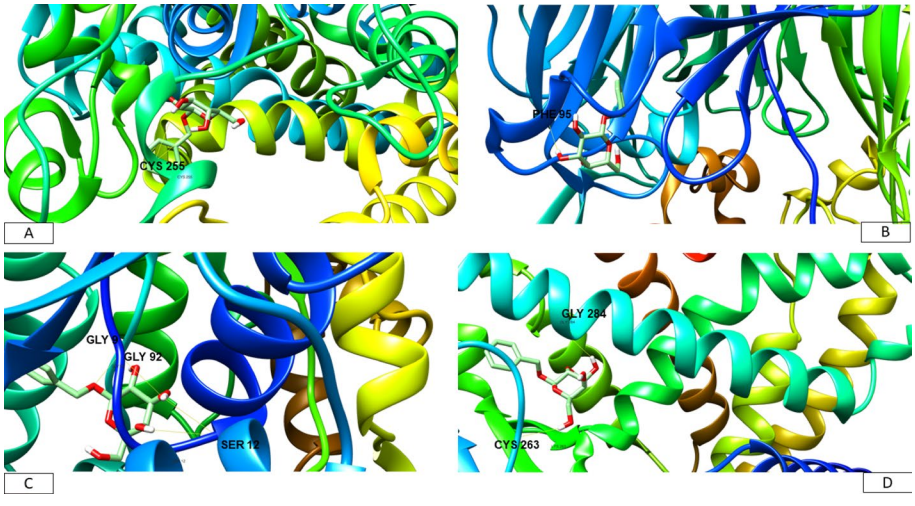

Fig. 3 A stable interaction between compound 15 and **A** 8hez, **B** 1j2e, **C** 1bhs, and **D** 1prg

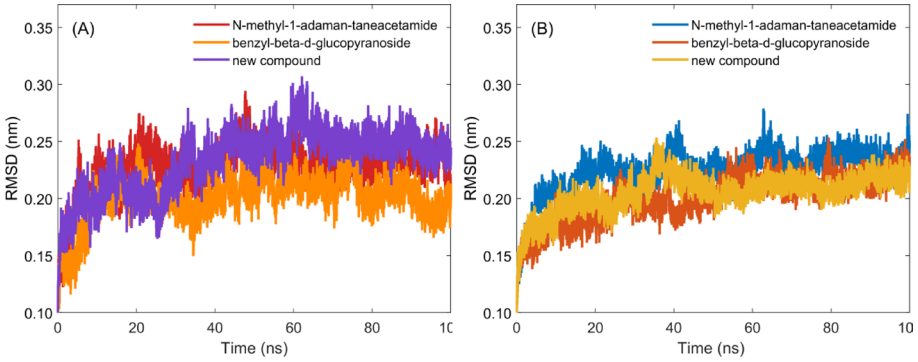

Fig. 4 The root mean squared standard deviation (RMSD) for diabetic receptors **A** Peroxisome proliferator-activated receptor (PPAR) and **B** Sodium-glucose cotransporter 2 (SGLT2), showing the stability and conformational changes over time with Benzyl β-D- glucopyranoside, 3′,4′-di-o-methyl ellagic acid-4α-l-rhamnopyranoside (new compound) and N-methyl-1-adamantaneacetamide

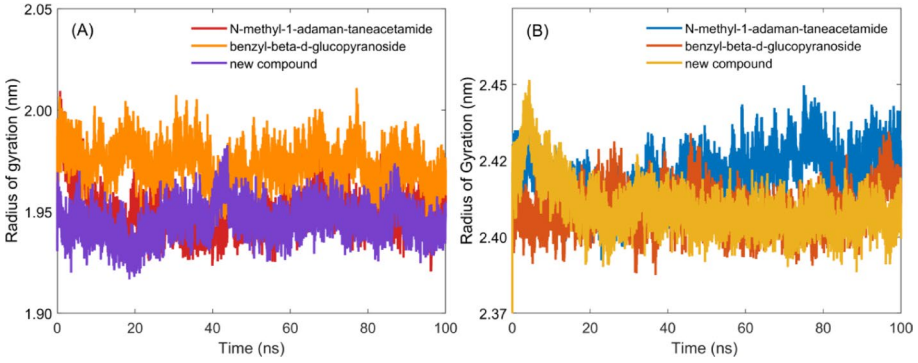

Fig. 5 The radius of gyration of diabetic receptors **A** Peroxisome proliferator-activated receptor (PPAR) and **B** Sodium-glucose cotransporter 2 (SGLT2), showing the structural compactness and overall stability with Benzyl β-D-glucopyranoside, 3′,4′-di-o-methyl ellagic acid-4α-l-rhamnopyranoside (new compound) and N-methyl-1-adamantaneacetamide

these ligands preserved the receptor's compact structure. Conversely, the benzyl β-D-glucopyranoside ligand caused the receptor to adopt an extended conformation with an increased Rg of 1.98 nm. This implies that the receptor underwent structural changes leading to a less compact and potentially less stable form when bound to the benzyl β-D-glucopyranoside ligand. Figure 5B shows that the new compound (3′,4′-di-O-methyl ellagic acid-4α-I-rhamnopyranoside) and benzyl β-D-glucopyranoside ligand maintained an Rg of 2.40 nm throughout the 100 ns simulation, indicating these ligands kept the receptor's compact structure. In contrast, the N-methyl-1-adamantaneacetamide ligand caused the receptor to adopt an extended conformation with Rg increasing to 2.42 nm. This suggests the receptor experienced structural changes resulting in a less compact and potentially less stable form when bound to the N-methyl-1-adamantaneacetamide ligand.

3.5.3 Root mean squared fluctuations

Root Mean Squared Fluctuation (RMSF) quantifies the flexibility of individual atoms or residues in a molecule, such as a protein, by measuring the average deviation of each from its mean position over time. It is used in molecular dynamics simulations to assess which parts of a protein are more dynamic or flexible, and which are more

stable. Figure 6A shows the RMSF profile for the nuclear receptor peroxisome proliferator-activated receptor, with most residues below 0.2 nm, except residues ranging from 245 to 270 and residue 440, which fluctuate at about 0.38 and 0.36 nm, respectively. In sodium-glucose cotransporter 2, most residues in systems with both ligands remain at lower fluctuations below 1.52 nm over 100 ns, with the new compound displaying the lowest fluctuations, indicating enhanced stability upon binding. Few residues exhibit fluctuations in both systems at 201 to 291 and 561 to 651. The fluctuations align with previously observed residues ASP21, ASN22, PRO246-ILE251, SER508-PHE520, and GLU569-ASP574, which show elevated fluctuations in the systems with dapagliflozin, canagliflozin, ipragliflozin, empagliflozin, tofogliflozin, and luseogliflozin [44].

3.6 Solvent accessible surface area

The solvent-accessible surface area (SASA) measures the surface area of a molecule, such as a protein, that is accessible to a solvent. It helps determine which parts of the molecule can interact with water or other solvents, providing insight into the molecule's structure and interactions with its environment. High SASA values generally indicate that a protein has many exposed regions, which can lead to decreased stability due to increased vulnerability to environmental factors such as solvent interactions and denaturation. Conversely, low SASA values suggest that the protein has fewer exposed areas, thus increasing stability. This is because the protein's core is more compact and protected from external influences, reducing the likelihood of structural disruptions. For the peroxisome proliferator-activated receptor (PPAR), the SASA values are displayed in Fig. 7A. Both systems' SASA values range from 145 to 155 nm^2. For benzyl β-D-glucopyranoside and the new compound, the SASA value decreases from 150 to 145 nm^2. A distinct pattern is observed with the N-methyl-1-adamantaneacetamide ligand: during the first 20 ns, the SASA decreases from 150 to 145 nm^2, followed by a drop to 140 nm^2 between 30 and 50 ns. Then, a sharp rise occurs from 60 to 80 ns, reaching 150 nm^2 and gradually decreasing to 145 nm^2 for the final 20 ns.

For benzyl β-D-glucopyranoside and the new compound, the SASA decreases from 150 to 145 nm^2, indicating that the protein becomes more stable as it adopts a more compact structure with fewer exposed regions. This suggests a stabilising effect of these ligands. In contrast, the N-methyl-1-adamantaneacetamide ligand induces a distinct

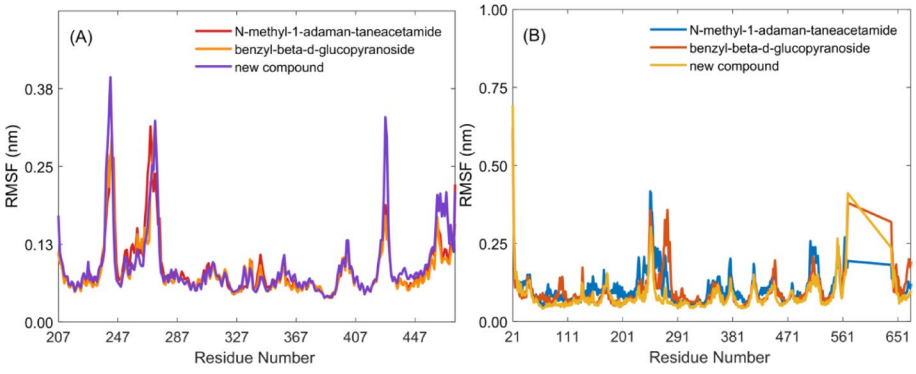

Fig. 6 The root mean square fluctuations of diabetic receptors: **A** Peroxisome proliferator-activated receptor (PPAR) and **B** Sodium-glucose cotransporter 2 (2GLT2), illustrating the flexibility and dynamic behaviou of residues with Benzyl β-D-glucopyranoside, 3′,4′-di-o-methyl ellagic acid-4α-l-rhamnopyranoside (new compound) and N-methyl-1-adamantaneacetamide

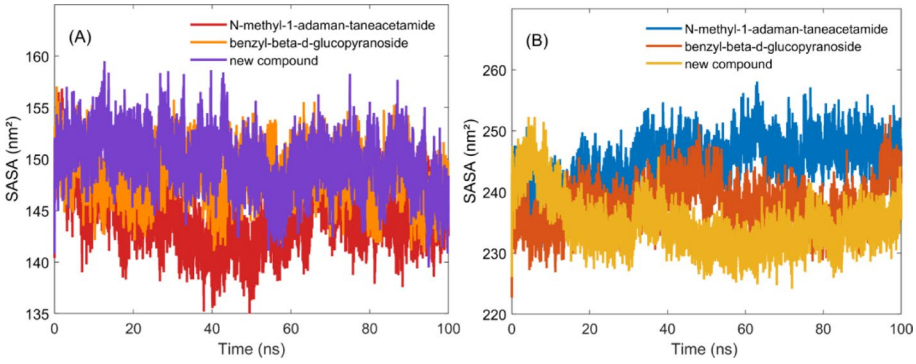

Fig. 7 Solvent-accessible surface area (SASA) of diabetic receptors: **A** Peroxisome proliferator-activated receptor (PPAR) and **B** Sodium-glucose cotransporter 2 (2GLT2), illustrating the accessible surface area to solvents during the binding event with Benzyl β-D-glucopyranoside, 3′,4′-di-o-methyl ellagic acid-4α-l-rhamnopyranoside (new compound) and N-methyl-1-adamantaneacetamide

pattern of SASA changes, with an initial decrease from 150 to 145 nm^2 and a further drop to 140 nm^2 at 30 and 50 ns. This is followed by a sharp rise to 150 nm^2 from 60 to 80 ns, gradually decreasing to 145 nm^2. These fluctuations imply that N-methyl-1-adamantaneacetamide causes significant conformational changes in PPAR, leading to dynamic rearrangements of the protein structure. Such behaviour suggests that this ligand induces transient stabilisation and exposure of different protein regions. In the sodium-glucose cotransporter, across two systems, a varied profile for SASA is observed in Fig. 7B. In the new compound, the SASA starts at 247 nm^2 in the first ten ns and then stabilises at 230 nm^2 for the remaining 90 ns. For the benzyl β-D-glucopyranoside system, the SASA profile remains at 246 nm^2 throughout the entire 100 ns, while in N-methyl-1-adamantaneacetamide, the surface area remains around 240 nm^2 throughout the timescale. Compared to the studied systems, the new compound exhibits the lowest SASA, indicating a successful reduction in the area accessible to solvent molecules and increased stability upon binding to the ligand.

3.7 Binding free energy calculations

The binding energy contributions between receptor peroxisome proliferator-activated receptor (PPAR) and sodium-glucose cotransporter 2 (SGLT2), as well as three ligands (N-methyl-1-adamantanecetamide, benzyl-β-D-glucopyranoside, and 3′,4′-di-O-methyl ellagic acid-4α-L-rhamnopyranoside), were analysed using MM/PBSA to calculate van der Waals and electrostatic energy contributions. The van der Waals, electrostatic, and total energies of the interactions are detailed in Table 6. The average binding energy components indicate strong and stable ligand attachment to the receptor, potentially harmful.

Compound 3′,4′-di-O-methyl ellagic acid-4α-L-rhamnopyranoside exhibits the strongest van der Waals and electrostatic interactions with both receptors. In the PPAR system, this ligand shows the lowest mean electrostatic energy contribution of -92.86 ± 12.00 kJ/mol and van der Waals contribution of -182.32 ± 11.49 kJ/mol, indicating a strong reliance on these components for PPAR binding. Furthermore, N-methyl-1-adamantaneacetamide has a van der Waals energy contribution of -115.83 ± 8.75 kJ/mol, and benzyl β-D-glucopyranoside has a binding energy of -142.18 ± 8.66 kJ/mol. The hierarchy of significance for both interactions in PPAR is

Table 6 Binding energy contributions of ligands with diabetes receptors PPAR and SGLT2

Binding energy contributions (kJ/mol)					
Ligands	**van der Waals**	**Electrostatic**	**Polar Solvation Energy**	**SASA energy**	**Binding Energy**
Peroxisome proliferator-activated receptor (PPAR)					
N-methyl-1-adamantaneacetamide	−115.83 ± 8.75	−16.80 ± 8.15	50.166 ± 9.21	−13.57 ± 0.64	−96.03 ± 9.75
Benzyl β-D-glucopyranoside	−142.18 ± 8.66	−21.82 ± 7.23	104.54 ± 10.48	−16.81 ± 0.83	−76.28 ± 9.51
3′,4′-di-o-methyl ellagic acid-4α-l-rhamnopyranoside	−182.32 ± 11.49	−92.86 ± 12.00	256.3 ± 19.38	−20.62 ± 0.98	−39.48 ± 15.85
Sodium-glucose cotransporter 2					
N-methyl-1-adamantaneacetamide	−56.23 ± 0.75	−17.23 ± 646	56.64 ± 13.47	−13.68 ± 1.23	−30.64 ± 17.38
Benzyl β-D-glucopyranoside	−109.91 ± 17.77	−115.859	228.42 ± 17.55	−16.82 ± 0.80	−14.17 ± 13.51
3′,4′-di-o-methyl ellagic acid-4α-l-rhamnopyranoside	−152.75 ± 15.19	−24.86 ± 864	102.24 ± 15.07	−15.82 ± 1.14	−91.19 ± 10.95

3′,4′-di-O-methyl ellagic acid-4α-L-rhamnopyranoside, benzyl β-D-glucopyranoside, and N-methyl-1-adamantaneacetamide.

When evaluating the total binding energy, other factors like polar solvation energy and solvent-accessible surface area (SASA) energy also contribute. Polar solvation energy generally opposes binding because of the desolvation penalty when a ligand attaches to a receptor, which results in positive values for this component. For example, 3′,4′-di-O-methyl ellagic acid-4α-L-rhamnopyranoside has a polar solvation energy of 256.3 ± 19.38 kJ/mol, significantly affecting the overall binding energy. Similarly, benzyl-β-D-glucopyranoside and N-methyl-1-adamantaneacetamide have polar solvation energies of 104.54 ± 10.48 kJ/mol and 50.166 ± 9.21 kJ/mol, respectively. The SASA energy, linked to hydrophobic interactions, also influences the total binding energy, though less so than van der Waals and electrostatic forces. For instance, 3′,4′-di-O-methyl ellagic acid-4α-L-rhamnopyranoside contributes −20.62 ± 0.98 kJ/mol, benzyl-β-D-glucopyranoside contributes −16.81 ± 0.83 kJ/mol, and N-methyl-1-adamantaneacetamide contributes −13.57 ± 0.64 kJ/mol.

Combining these contributions, the total binding energies for the ligands in the PPAR system are: 3′,4′-di-O-methyl ellagic acid-4α-L-rhamnopyranoside: −39.48 ± 15.85 kJ/mol, Benzyl-β-D-glucopyranoside: −76.28 ± 9.51 kJ/mol, and N-methyl-1-adamantaneacetamide: − 96.03 ± 9.75 kJ/mol. Despite its strong van der Waals and electrostatic interactions, the substantial positive polar solvation energy lowers the binding affinity of 3′,4′-di-O-methyl ellagic acid-4α-L-rhamnopyranoside. In contrast, the lower polar solvation energy of N-methyl-1-adamantaneacetamide boosts its overall binding energy, making it the ligand with the most favourable total binding energy in the PPAR system.

For the SGLT2 receptor, 3′,4′-di-O-methyl ellagic acid-4α-L-rhamnopyranoside shows the highest binding energy contributions, with van der Waals interaction of − 152.75 ± 15.19 kJ/mol and an electrostatic energy of − 24.86 ± 8.64 kJ/mol. Benzyl-β-D-glucopyranoside follows with van der Waals and electrostatic energies of − 109.91 ± 17.77 kJ/mol and − 115.85 ± 9.00 kJ/mol, respectively. N-methyl-1-adamantanecetamide has the lowest contributions, with van der Waals and electrostatic energies of − 56.23 ± 0.75 kJ/mol and − 17.23 ± 6.46 kJ/mol. The polar solvation energy for 3′,4′-di-O-methyl ellagic acid-4α-L-rhamnopyranoside is 102.24 ± 15.07 kJ/

mol, while for benzyl-β-D-glucopyranoside and N-methyl-1-adamantanecetamide, it is 228.42 ± 17.55 kJ/mol and 56.64 ± 13.47 kJ/mol, respectively. SASA energies are − 15.82 ± 1.14 kJ/mol for 3′,4′-di-O-methyl ellagic acid-4α-L-rhamnopyranoside, − 16.82 ± 0.80 kJ/mol for Benzyl-β-D-glucopyranoside, and -13.68 ± 1.23 kJ/mol for N-methyl-1-adamantanecetamide. The total binding energies for these ligands in the SGLT2 system are − 91.19 ± 10.95 kJ/mol, − 14.17 ± 13.51 kJ/mol, and − 30.64 ± 17.38 kJ/mol, respectively. 3′,4′-di-O-methyl ellagic acid-4α-L-rhamnopyranoside enhances its overall binding energy, making it the ligand with the most favourable total binding energy in the SGLT2 system.

4 Discussion

Type 2 diabetes is characterised by high blood sugar (blood glucose) levels, which cause severe damage to the heart, blood vessels, kidneys, nerves, and eyes. It usually affects adults and results from insufficient or resistant insulin production in the body [45]. Managing type 2 diabetes involves a combination of lifestyle changes, such as a healthy diet, regular exercise, weight management, and limited alcohol intake, alongside medication that lowers blood sugar levels through different mechanisms, such as metformin, sulfonylureas, DPP-4 inhibitors, SGLT-2 inhibitors, and GLP-1 receptor agonists [46]. Sometimes, insulin therapy becomes necessary, with individuals with type 2 diabetes eventually requiring insulin injections or an insulin pump to control blood sugar levels better [47]. Understanding novel therapeutic targets and blood sugar-controlling medications with fewer side effects and higher efficacy is vital for managing blood sugar disorders. This has driven research into identifying natural compounds from *A. gangetica* and *S. glaucescens*, which may serve as therapeutic targets for blood sugar regulation using computer-aided drug discovery tools. e blood sugar using computer-aided drug discovery tools.

ADME (absorption, distribution, metabolism, and excretion) profiling is essential in drug discovery and development to assess a compound's pharmacokinetic properties and potential. Based on the results, Log Po/w (partition coefficient) indicates a compound's lipophilicity. Higher Log Po/w values, such as those observed in compounds 2, 3, 4, 10, 11, and 13, suggest increased lipophilicity, influencing their absorption and distribution in the body. Log S reflects a compound's aqueous solubility; lower Log S values, seen with compounds 2, 3, 4, 7, 8, 10, 11, 12, 13, and 14, indicate decreased solubility, potentially affecting bioavailability and absorption [48]. GI absorption predicts the likelihood of a compound being absorbed in the gastrointestinal tract. Compounds labelled "High" are expected to be well absorbed, whereas those marked "Low" exhibit reduced absorption rates. BBB (blood–brain barrier permeability) is vital for drugs targeting the central nervous system. Compounds marked "Yes," such as 2, 3, 4, 8, 10, and 11, show potential for crossing the blood–brain barrier, which is essential for central nervous system drugs [48]. P-glycoprotein (P-gp) is an efflux transporter that limits drug absorption. Compounds marked "Yes" may be substrates for P-gp, possibly affecting their bioavailability and vice versa. Inhibition of P-gp can increase a drug's bioavailability by reducing its efflux from the intestinal wall, thereby enhancing efficacy. However, this could also raise toxicity and adverse effects, as higher drug concentrations might accumulate. CYP inhibition (cytochrome enzymes) is a key aspect of drug metabolism. Those marked "Yes" for CYP inhibition, such as compounds 2, 3, and 11, might inhibit specific

CYP enzymes, potentially leading to drug-drug interactions. While CYP inhibition can enhance bioavailability, prolong the drug's duration of action, and allow dose reduction, it also carries risks of altered metabolism and interactions, depending on treatment aims, pharmacokinetics, and patient factors [49].

In diabetes, two target and ligand interactions were examined. We recorded the binding scores (kcal/mol) for various compounds against four targets (8hez, 1j2e, 1bhs, 1prg), obtained through Chimera and Autodock Vina. A more negative score indicated a stronger interaction between the ligand and the protein. For example, compounds 7, 12, and 13 demonstrated the most negative scores across all targets compared to the standards, as shown in Table 5, indicating a potential strong binding interaction. Moreover, compounds 7 and 12 displayed higher activity, suggesting their potential as biologically active compounds. The greater the activity, the stronger the pharmacological effects or the potential for these compounds to be promising drug candidates.

While compounds 7 and 12 showed high docking scores, their poor ADME profiles suggest limited oral bioavailability. Nanoformulation or structural optimisation may enhance their therapeutic potential, as presented in Table 3. Compound 14, although not indexed in PubChem or ChEMBL, shares structural features with known antidiabetic ellagic acids and warrants further investigation. Nevertheless, various ellagic acids have demonstrated therapeutic effects against type 2 diabetes induced by streptozotocin in rats. Moreover, the Nano formulation of ellagic acids has been found to provide an effective diabetes treatment, which improves their oral bioavailability [50, 51]. The pharmacokinetic properties of ellagic acids, including compound 14 isolated from *S. glaucescens pax* [11], contribute to their nanoformulation as indicated in Table 3. The diabetic activity of some ellagic acids favors compound 14 to be searched as a type 2 diabetic drug. Therefore, SwissTargetPrediction and ChEMBL predictions were cross-validated using probability thresholds and known actives. While experimental validation is pending, the in-silico findings provide a strong rationale for future in vitro and in vivo studies.

In Fig. 4, the RMSD profiles were comparable to those of previously studied inhibitors targeting similar type 2 diabetes receptors, such as the pioglitazone inhibitor, which exhibited RMSD values around 0.2 nm. Interestingly, the RMSD values of benzyl β-D-glucopyranoside, 3′,4′-di-o-methyl ellagic acid-4α-I-rhamnopyranoside, and N-methyl-1-adamantaneacetamide compounds were higher than those of the rosiglitazone inhibitor, which had an average RMSD of 0.35 nm. The observations suggest that the studied inhibitors sustain greater receptor stability than the rosiglitazone inhibitor, which is associated with increased structural flexibility or instability with PPAR diabetic type 2 receptors.

For the sodium-glucose cotransporter 2 (SGLT2) receptor, the RMSD profiles observed in Fig. 1B ranged from 0.20 to 0.25 nm. 3′,4′-di-o-methyl ellagic acid-4α-I-rhamnopyranoside (new compound) showed the lowest and most stable RMSD, maintaining a distance of 0.20 nm, similar to the benzyl β-D-glucopyranoside ligand. As mentioned earlier, the N-methyl-1-adamantaneacetamide ligand exhibited a higher RMSD than the other ligands.

Figure 6 in the study, the fluctuation of two diabetic targets has been examined, and the highest fluctuations involve a loop connecting helix strands and beta sheets in the residue range of 245. This finding aligns with previous studies, including those investigating rosiglitazone interactions with Pparγ. NMR spectroscopy has shown that Pparγ

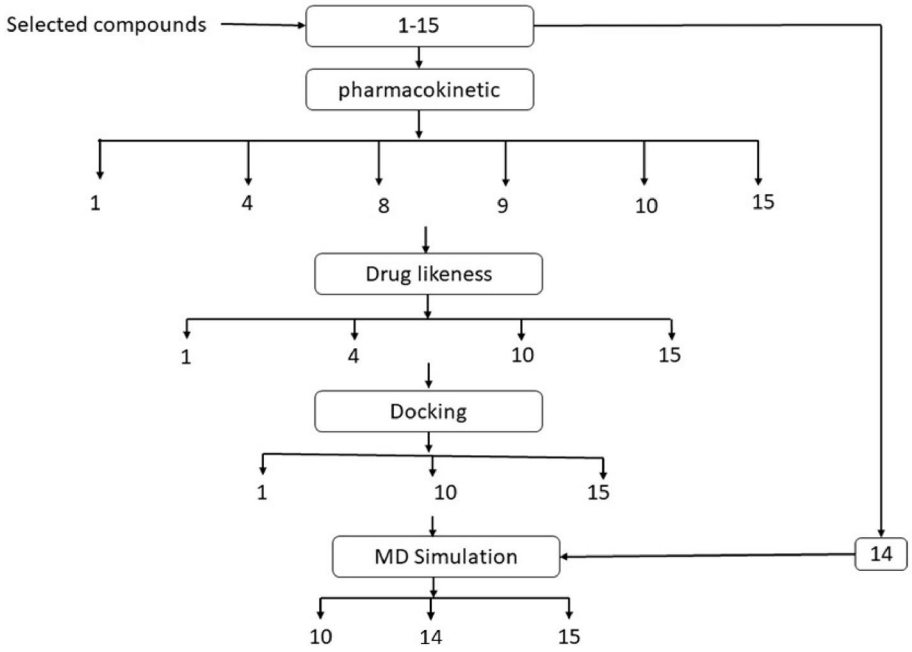

Fig. 8 Selection of favorable oral bioavailability compound

is highly dynamic, especially at the Ω-loop (connecting H2 and H3), which is part of the ligand-binding domain. These studies have associated potency with ligand interactions involving aliphatic and polar groups in this region, which is consistent with the presence of polar groups in our ligands. The head groups of rosiglitazone and pioglitazone form hydrogen bond networks with polar residues, stabilising H12 and AF2 in Pparγ. Consequently, a 100 ns simulation duration was adequate to observe conformational stability, as indicated by consistent RMSD and Rg values. Comparison with standard drugs (e.g., pioglitazone, rosiglitazone) validated the reliability of the observed dynamics. Nevertheless, the absence of control simulations (protein alone) is a limitation.

In Table 6 the varying energy contributions corresponding to different structures are observed, and most interactions are affected by the functional and structural attributes of the compounds. N-methyl-1-adamantaneacetamide has a binding energy contribution of -115.83 ± 8.75 kJ/mol, attributed to its hydrophobic adamantane core, which maximises contact with the receptor's hydrophobic pockets. Benzyl β-D-glucopyranoside, with a binding energy of -142.18 ± 8.66 kJ/mol, features an aromatic benzyl group that enables π–π stacking interactions, enhancing its binding affinity. The highest binding energy, -182.32 ± 11.49 kJ/mol, is observed with 3′,4′-di-O-methyl ellagic acid-4α-I-rhamnopyranoside, whose multiple fused aromatic rings and methyl groups facilitate extensive van der Waals interactions within the receptor's binding pocket. These findings align with studies of similar receptors, where compounds like gusperimus and miltefosine demonstrate structural features that enhance hydrophobic interactions. Gusperimus's long hydrocarbon chains, amphiphilic nature, and strong van der Waals forces facilitate effective interactions in lipid environments. Similarly, miltefosine's hydrophobic alkyl chain and its ability to integrate into lipid bilayers ensure robust interactions within hydrophobic domains.

The activities carried out during this study are outlined in Fig. 8, prioritising compounds with advantageous oral bioavailability related to pharmacokinetics and

drug-likeness for further examination. Initially, 15 compounds were selected and appraised for drug-likeness and pharmacokinetic traits. The compounds exhibiting the most favourable pharmacokinetic profiles were further targeted against four receptors associated with type 2 diabetes using molecular docking, and their stability was evaluated through molecular dynamics simulations. The highest binding energy was recorded with N-methyl-1-adamantaneacetamide, which displayed a PPARγ binding energy of − 115.83 ± 8.75 kJ/mol, and 3′,4′-di-O-methyl ellagic acid–4α-L-rhamnopyranoside with − 152.75 ± 15.19 kJ/mol for SGLT2 (Table 6). MD trajectories over 100 ns showed stable RMSD values (0.20–0.30 nm), consistent Rg patterns, and low SASA fluctuations, similar to those observed in rosiglitazone and empagliflozin complexes. These findings indicate strong van der Waals interactions complemented by beneficial electrostatic forces. Polar solvation penalties were moderate, especially for the adamantane derivative, resulting in overall binding energies of − 96.03 ± 9.75 kJ/mol (PPARγ) and − 91.19 ± 10.95 kJ/mol (SGLT2). In silico predictions must be confirmed through experimental validation. Future research will include enzyme inhibition assays and glucose uptake experiments in cell models.

5 Conclusion

This study used in silico methods to assess phytochemicals from *Asystasia gangetica* and *Synadenium glaucescens pax* for their potential as antidiabetic agents. N-methyl-1-adamantaneacetamide and 3′,4′-di-O-methyl ellagic acid-4α-L-rhamnopyranoside showed favourable binding affinities, pharmacokinetic properties, and molecular stability against PPARγ and SGLT2 receptors, respectively. While these results indicate promising therapeutic potential, they are preliminary and based solely on computational predictions. Experimental validation—including in vitro and in vivo tests—is vital to confirm efficacy, safety, and mechanisms of action. These compounds could serve as lead candidates for future drug development targeting type 2 diabetes mellitus.

Abbreviations

A	Active
I	Inactive
E	Empty
B	Both
Hs	Homo sapiens
Rn	*Rattus norvegicus*
PPARγ	Peroxisome proliferator activated receptor gamma
DPP4	Dipeptidyl peptidase IV
SGLT-2	Sodium-glucose transport protein 2
11β-HS1	11ββ-hydroxysteroid dehydrogenase 1
ADME	Absorption, distribution, metabolism, and excretion
MD Simulation	Molecular dynamic simulation
NVT	Number of particles, system volume, and temperature
NPT	Number of particles, system pressure, and temperature

Supplementary Information

The online version contains supplementary material available at https://doi.org/10.1007/s44395-025-00036-y.

Supplementary Material 1.

Acknowledgements
Not applicable.

Author contributions

Conceptualisation, techniques, data curation, first draft writing, writing review, and editing were all carried out by NMK. Methodology, formal analysis, and writing, including review and editing, fell under the responsibility of CJM. FPM's

contributions to conceptualisation, methodology, formal analysis, and writing, including review and editing, were subject to review process and editing.

Funding
No financial support for the research.

Data availability
The authors declare that the data supporting the findings of this study are available within the paper and its supplementary data files. Any raw data files be needed in another format, they are available from the corresponding author upon reasonable request. Source data are provided with this paper.

Declarations

Ethics approval and consent to participate
Not applicable.

Consent for publication
Not applicable.

Competing interests
The authors declare that they have no competing interests.

Received: 27 April 2025 / Accepted: 23 December 2025
Published online: 29 January 2026

References

1. Sun X, Yu W, Hu C. Genetics of type 2 diabetes: insights into the pathogenesis and its clinical application. BioMed Res Int. 2014. https://doi.org/10.1155/2014/926713.
2. Saisho Y. Importance of beta cell function for the treatment of type 2 diabetes. J Clin Med. 2014;3(3):923–43.
3. International Diabetes Federation. Annual Report; 2023.
4. Belete TM. A recent achievement in the discovery and development of novel targets for the treatment of type-2 diabetes mellitus. J Exp Pharmacol. 2020. https://doi.org/10.2147/JEP.S226113.
5. Webber S. International diabetes federation. Diabet Res Clin Pract. 2021;102(2):147–8. https://doi.org/10.1016/j.diabres.2013.10.013.
6. Abiola O, Abiola A, Okikiola D, Ayodeji F. Informatics in medicine unlocked GC-MS and molecular docking studies of *Hunteria umbellata* methanolic extract as a potent anti-diabetic. Inform Med Unlocked. 2018;13:1–8. https://doi.org/10.1016/j.imu.2018.08.001.
7. Ahmed HA, Alkali IY, Mahmud AF. In silico molecular docking studies of some phytochemicals against dipeptidyl peptidase 4. Int Res J of Pharm Med Sci. 2018;1(6):65–8.
8. Damián-Medina K, Salinas-Moreno Y, Milenkovic D, Figueroa-Yáñez L, Marino-Marmolejo E, Higuera-Ciapara I, et al. In silico analysis of antidiabetic potential of phenolic compounds from blue corn (*Zea mays* L.) and black bean (*Phaseolus vulgaris* L.). Heliyon. 2020. https://doi.org/10.1016/j.heliyon.2020.e03632.
9. Hariprasad MMVRTPN. In silico analysis of a potential antidiabetic phytochemical erythrin against therapeutic targets of diabetes. In Silico Pharmacol. 2021. https://doi.org/10.1007/s40203-020-00065-8.
10. Sama K. Pharmacognostical and phytochemical screening of *Asystasia gangetica* (Chinese violet). Int Res J Pharm. 2013;4:161–3.
11. Rwegoshora F, Mabiki F, Machumi F, Chacha M, Styrishave B, Cornett C. A new ellagic acid rhamnoside from *Synadenium glaucescens* and its cytotoxicity evaluation. Chem Nat Compd. 2023;59(4):670–4.
12. Sama K, Sivaraj R, Rajiv P. In vitro antidiabetic activity of anthocyanin extract of *Asystasia gangetica* (Chinese violet) flower. Asian J Plant Sci Res. 2013;3(2):88–92.
13. Credo D, Cornett C, Mabiki F. Anti-Newcastle disease virus activity of 3β and 3α friedelanol triterpenoids from the leaves of *Synadenium glaucescens* Pax. Trop Biomed. 2022;39(2):257–64. https://doi.org/10.47665/tb.39.2.016.
14. Credo D, Mabiki FP, Machumi F, Chacha M, Cornett C, Styrishave B. Anti-Newcastle disease virus activity of 3β and 3α friedelanol triterpenoids from the leaves of *Synadenium glaucescens* Pax. Trop Biomed. 2022;39(2):257–64. https://doi.org/10.47665/tb.39.2.016.
15. Mabiki F, Mdegela R, Mosha R, Magadula J. Antiviral activity of crude extracts of *Synadenium glaucescens* (Pax) against infectious bursal disease and fowlpox virus. J Med Plant Res. 2013;7(14):871–6. https://doi.org/10.5897/JMPR12.777.
16. Mabiki FP, Magadula JJ, Mdegela RH, Mosha RD. Optimization of extraction conditions and phytochemical screening of root extract of *Synadenium glaucescens* Pax. Int J Chem. 2013;5(4):103–12. https://doi.org/10.5539/ijc.v5n4p103.
17. Mary OG, Zaituni MS, Faith MP, Lughano KJM, Robinson MH, John OE. Antibacterial effects of single and combined crude extracts of *Synadenium glaucescens* and *Commiphora swynnertonii*. Afr J Infect Dis. 2022;16(2 Suppl):9–16.
18. Msengwa Z, Credo D, Mafuru M, Mwesongo J, Mabiki FP, Mwang'onde BJ, et al. Bacteriostatic and haemolytic activities of extracts and compounds of *Commiphora swynnertonii*. Res J Pharmacogn. 2023;10(2):47–56. https://doi.org/10.22127/RJP.2023.370231.2009.
19. Herrera-ceu UC, Univer- CEU. A pharmacological update of ellagic acid authors. Planta Med. 2018;84:1068–93.
20. Oluwaseyi Famuyiwa S, Olatubosun Faloye K, Durojaiye Ayoola M, Gabriel Fakola E, Tantoh Ndinteh D. 4′-O-galloy-3,3′-di-O-methylellargic acid 4-O-xylopyranoside; a potential anti-diabetic agent. Results Chem. 2022;4:100644. https://doi.org/10.1016/j.rechem.2022.100644.
21. Genovese M. New perspective on type 2 diabetes and obesity treatment: study and development of new natural/synthetic inhibitors of tyrosine phosphatase 1B (PTP1B); 2023

22. Teimouri M, Hosseini H, ArabSadeghabadi Z, Babaei-Khorzoughi R, Gorgani-Firuzjaee S, Meshkani R. The role of protein tyrosine phosphatase 1B (PTP1B) in the pathogenesis of type 2 diabetes mellitus and its complications. J Physiol Biochem. 2022;78:307–22.
23. Batista TM, Haider N, Kahn CR. Defining the underlying defect in insulin action in type 2 diabetes. Diabetologia. 2021;64:994–1006.
24. Haye A, Ansari MA, Rahman SO, Shamsi Y, Ahmed D, Sharma M. Role of AMP-activated protein kinase on cardio-metabolic abnormalities in the development of diabetic cardiomyopathy: a molecular landscape. Eur J Pharmacol. 2020;888:173376.
25. Gregory S, Hill D, Grey B, Ketelbey W, Miller T, Muniz-Terrera G, et al. 11β-hydroxysteroid dehydrogenase type 1 inhibitor use in human disease-a systematic review and narrative synthesis. Metabolism. 2020;108:154246.
26. Berger C, Zdzieblo D. Glucose transporters in pancreatic islets. Pflugers Arch-Eur J Physiol. 2020;472(9):1249–72.
27. Mishra BK, Banerjee BD, Agrawal V, Madhu SV. Association of PPAR γ gene expression with postprandial hypertriglyceridaemia and risk of type 2 diabetes mellitus. Endocrine. 2020;68:549–56.
28. Kondo M, Tahara A, Hayashi K, Inami H, Ishikawa T, Tomura Y. Therapeutic effects of interleukin-1 receptor-associated kinase 4 inhibitor AS2444697 on diabetic nephropathy in type 2 diabetic mice. Naunyn-Schmiedebergs Arch Pharmacol. 2020;393(7):1197–209.
29. Xu Y, Huang Y, Song R, Ren Y, Chen X, Zhang C, et al. Development of disulfide-derived fructose-1, 6-bisphosphatase (FBPase) covalent inhibitors for the treatment of type 2 diabetes. Eur J Med Chem. 2020;203:112500.
30. Deacon CF. Dipeptidyl peptidase 4 inhibitors in the treatment of type 2 diabetes mellitus. Nat Rev Endocrinol. 2020;16(11):642–53.
31. Oliveira IA, Allonso D, Fernandes TVA, Lucena DMS, Ventura GT, Dias WB, et al. Enzymatic and structural properties of human glutamine: fructose-6-phosphate amidotransferase 2 (hGFAT2). J Biol Chem. 2021. https://doi.org/10.1074/jbc.RA120.015189.
32. Provenzano M, Pelle MC, Zaffina I, Tassone B, Pujia R, Ricchio M, et al. Sodium-glucose co-transporter-2 inhibitors and nephroprotection in diabetic patients: more than a challenge. Front Med. 2021;8:654557.
33. Kumar H, Ishu, Singh H. *Asystasia gangetica*: a bibliometric assessment of global publications output during 1960–2020. Int J Pharm Sci Res. 2013;12(4):12–26. https://doi.org/10.13040/IJPSR.0975-8232.12(4).2021-35.
34. Daina A, Michielin O, Zoete V. SwissADME: a free web tool to evaluate pharmacokinetics, drug-likeness and medicinal chemistry friendliness of small molecules. Sci Rep. 2017;7(1):42717.
35. Abraham MJ, Murtola T, Schulz R, Páll S, Smith JC, Hess B, et al. GROMACS: high performance molecular simulations through multi-level parallelism from laptops to supercomputers. SoftwareX. 2015;1:19–25.
36. Aci-Sèche S, Genest M, Garnier N. Ligand entry pathways in the ligand binding domain of PPARγ receptor. FEBS Lett. 2011;585(16):2599–603.
37. Bruning JB, Chalmers MJ, Prasad S, Busby SA, Kamenecka TM, He Y, et al. Partial agonists activate PPARγ using a helix 12 independent mechanism. Structure. 2007;15(10):1258–71.
38. Mark P, Nilsson L. Structure and dynamics of the TIP3P, SPC, and SPC/E water models at 298 K. J Phys Chem A. 2001;105(43):9954–60.
39. Bryson AE, Denham WF. A steepest-ascent method for solving optimum programming problems. J Appl Mech. 1962. https://doi.org/10.1115/1.3640537.
40. Parrinello M, Rahman A. Polymorphic transitions in single crystals: a new molecular dynamics method. J Appl Phys. 1981;52(12):7182–90.
41. Hess B, Bekker H, Berendsen HJC, Fraaije JGEM. LINCS: a linear constraint solver for molecular simulations. J Comput Chem. 1997;18(12):1463–72.
42. Hasan T, Islam A, Rahman N, Ahmed S, Islam A, Ud AFMS. Phytochemicals from *Zingiber capitatum* rhizome as potential a—glucosidase , a -amylase , and glycogen phosphorylase inhibitors for the management of Type-II diabetes mellitus: inferences from in - vitro , in-vivo and in-silico investigations. Arab J Chem. 2023;16(10):105128. https://doi.org/10.1016/j.arabjc.2023.105128.
43. Zhao M, Ma J, Li M, Zhang Y, Jiang B, Zhao X, et al. Cytochrome p450 enzymes and drug metabolism in humans. Int J Mol Sci. 2021;22(23):1–16. https://doi.org/10.3390/ijms222312808.
44. Kong J, Li L, Yuan H, Bai F, Yang K, Zhao L, et al. In silico discovery of potential sodium–glucose cotransporter-2 inhibitors from natural products for treatment of heart failure via molecular docking and molecular dynamics simulation approach. J Biomol Struct Dyn. 2023;41(17):8109–20.
45. Chan M. Global report on diabetes. vol. 978, 2016, pp. 6–86. https://www.who.int/publications/i/item/9789241565257
46. Ganesan K, Rana MBM, Sultan S. Oral hypoglycemic medications; 2018.
47. Procaccini M, Allegra AG, Burns D, Sisson E. Using insulin pump for glycemic control in patients with severe insulin resistance. J Am Pharm Assoc. 2024. https://doi.org/10.1016/j.japh.2024.01.003.
48. Rocha B, de Morais LA, Viana MC, Carneiro G. Promising strategies for improving oral bioavailability of poor water-soluble drugs. Expert Opin Drug Discov. 2023;18(6):615–27.
49. Zhu S, Bai Q, Li L, Xu T. Drug repositioning in drug discovery of T2DM and repositioning potential of antidiabetic agents. Comput Struct Biotechnol J. 2022;20:2839–47. https://doi.org/10.1016/j.csbj.2022.05.057.
50. Harakeh S, Almuhayawi M, Jaouni SA, Almasaudi S, Hassan S, Amri TA, et al. Antidiabetic effects of novel ellagic acid nanoformulation: insulin-secreting and anti-apoptosis effects. Saudi J Biol Sci. 2020;27(12):3474–80. https://doi.org/10.1016/j.sjbs.2020.09.060.
51. Malini P, Kanchana G, Rajadurai M. Antibiabetic efficacy of ellagic acid in streptozotoc-ininduced diabetes mellitus in albino wistar rats. Asian J Pharm Clin Res. 2011;4(3):124–8.

Publisher's Note